J Mater Sci (2008) 43:88–97
DOI 10.1007/s10853-007-2136-2

Interface layer effect on the stress distribution of a wafer-bonded bilayer structure

Yin Zhang

Received: 14 September 2006 / Accepted: 30 August 2007 / Published online: 26 September 2007

Abstract The interface layer plays an important role in stress transfer in composite structures. However, many interface layer properties such as the modulus, thickness, and uniformity are difficult to determine. The model developed in this article links the influence of the interface layer on the normal stress distribution along the layer thickness with the layer surface morphology before bonding. By doing so, a new method of determining the interfacial parameter(s) is suggested. The effects of the layer thickness and the surface roughness before bonding on the normal stress distribution and its depth profile are also discussed. For ideal interface case with no interfacial shear stress, the normal stress distribution pattern can only be monotonically decreased from the interface. Due to the presence of interfacial shear stress, the normal stress distribution is much more complex, and varies dramatically with changes in the properties of the interface layer, or the dimensions of the bonding layers. The consequence of this dramatic stress field change, such as the shift of the maximum stress from the interface is also addressed. The size-dependent stress distribution in the thickness direction due to the interface layer effect is presented. When the interfacial shear stress is reduced to zero, the model presented in this article is also demonstrated to have the same normal stress distribution as obtained by the previous model, which does not consider the interface layer effect.

Y. Zhang (✉)
State Key Laboratory of Nonlinear Mechanics (LNM), Institute of Mechanics, Chinese Academy of Sciences, Beijing 100080, P.R. China
e-mail: zhangyin@lnm.imech.ac.cn

Introduction

Both experimental studies and approximate analytical solutions [1–6] indicate complex stress states with a rapid gradient occurring along the edges of composite structures. Thus, the so called boundary effects or edge-induced stress phenomena have been intensively investigated. These effects result from the presence and interaction of geometric and material discontinuities through the laminate thickness [5]. Almost all solid-state electronic components have the basic composite structure of a substrate with one or multiple film overlays [7]. Therefore the stress distribution due to the geometric and material discontinuities is of great concern for electronic components manufacturing, processing, and reliability. An excellent and comprehensive review article on this issue is given by Hu [8].

Interface layer models including the shear–lag (S–L)model [9] and the lap–shear (L–S) model [10, 11] have been developed as a supplement/improvement to the Timoshenko model of bimetal thermostat bending induced by temperature [12]. The Timoshenko model offers overall bending information for a composite structure and the longitudinal force inside the layers, but provides no information about the interfacial stresses, which dominate the failure of multilayered materials [13]. Geometrically, the Timoshenko model deals with composite layers with finite width and thickness, but infinite length. The longitudinal normal stress distribution due to temperature difference predicted by the S–L model is given as follows [9], which deviates significantly from that predicted by the Timoshenko model when the sample size reduces to the scale of micron [14],

$$\sigma_{xx}^{f} \sim E_f \Delta T(\alpha_f - \alpha_s)\left[\frac{\cosh(\beta x)}{\cosh(\beta l)} - 1\right],$$
$$\beta \propto \sqrt{\frac{G_i}{\eta}\left(\frac{1}{E_f t_f} + \frac{1}{E_s t_s}\right)}. \quad (1)$$

σ_{xx}^{f} is the film longitudinal stress. E_f , E_s and α_f , α_s are the effective Young's moduli and coefficients of thermal expansion of the film and substrate, respectively. t_f and t_s are the thickness of the film and substrate. l is half of the film length. ΔT is the temperature deviation from the temperature, at which the composite is in a zero stress state. G_i and η are the shear modulus and thickness of the interface layer, respectively. As indicated in Eq. 1 the interfacial parameter $\frac{G_i}{\eta}$ along with bilayer elastic moduli and dimensions determines the stress distribution. Originally $\frac{G_i}{\eta}$ was designed to account for the adhesiveness/bondedness at the layer interface, i.e., to provide a simple path for introducing a non-ideal interface into the model [14]. Mathematically, $\frac{G_i}{\eta}$ is a fitting factor. However, a method to physically evaluate G_i or η is not provided in those interface layer models. Without explicitly specifying the parameter of $\frac{G_i}{\eta}$, the S–L model cannot predict even the simplest case of the thermo-mechanical response of layered structures [14]. Also, as a fitting factor, $\frac{G_i}{\eta}$ can disguise the true nature of stress transfer between the film and substrate [14]. The dilemma is that such an interface layer does exist physically, but little is known about its uniformity, thickness, and elastic modulus [14]. The S–L model is thus advised to be used with caution, preferably after experimental verification [14]. The way out of this dilemma suggested by Murray and Noyan, [14, 15], is to develop a more comprehensive model which captures not only the stress transfer nature of the film–substrate interface but also the information of both the near (to the interface) and remote parts of the substrate, which may be significantly thicker than the film. Experimentally, the parameter $\frac{G_i}{\eta}$ changes due to interface evolution during thermal processing [14]. Therefore, different interface states match different $\frac{G_i}{\eta}$ values, and this should be reflected by some physical parameters, which is the goal this article aims to achieve. This article presents a model to link $\frac{G_i}{\eta}$ with the normal stress distribution in the layer thickness direction.

In the field of wafer bonding, the effect of surface roughness on bonding has been widely studied. Maszara et al. experimentally observed a periodic strain field near the interface of a bonded pair of silicon wafers [16]. Their X-ray topography (XRT) images clearly differentiate the bonded areas and unbonded "voids". The surface waviness/roughness represented schematically in Fig. 1a and b is responsible for the periodic strain field [16]. The closing

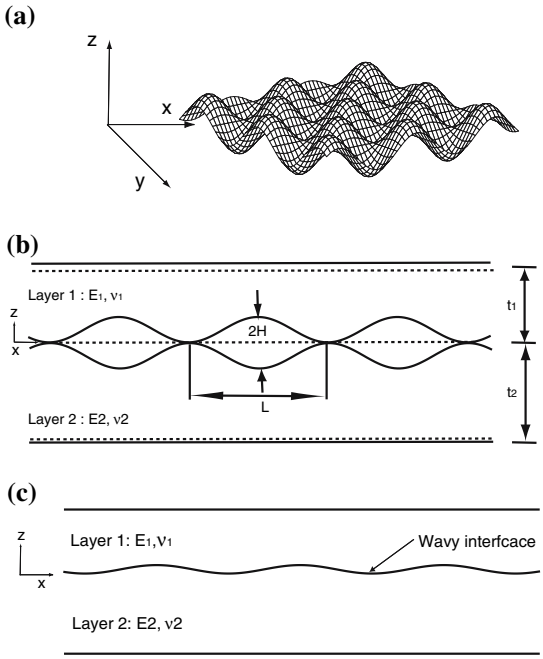

Fig. 1 (**a**) Schematic diagram of sinusoidally varying interface and the coordinate system. (**b**) The cross-section normal to the interface and layer dimensions. (**a**) and (**b**) are after reference [19]. (**c**) The final contact state: fully-bonded state

gap model, initially proposed by Stengl et al. [17], was further developed by Tong and Gösele [18]. On the basis of the model of Tong and Gösele, Yu and Suo did a comprehensive study on this closing gap model, and gave the critical misfit gap amplitude for the full bonding of two wafers [19]. It is worth pointing out that by constructing a delicate displacement field, the model of Yu and Suo [19] offers analytical close-form solutions for both the stress and displacement in bonded wafers. Before we go any further to other topics, let us briefly discuss how the closing gap model works. When the Dupré work of adhesion is positive (and it is positive for most cases), combining two free surfaces into an interface reduces the net free energy [19]. As illustrated in Fig. 1b, when the two layers are brought together, there are only small contact areas. Therefore, both the free areas and the free energy are large. At this stage, the Dupré work of adhesion is the driving mechanism to bring the two layers into contact, forming the interface, and reducing the free energy. However, when the layers elastically deform to contact, it increases the elastic energy. So the competition between the energy increase due to layer-accommodating elastic deformation and the energy decrease due to interface formation determines the final contact state of the two layers. For a small misfit gap, the two layers may be bonded completely when the total energy increase due to elastic deformation is less than the total energy decrease due to interface formation. For the large misfit gap case, a large elastic deformation is required to

contact, and thus there will be too much elastic energy increase for the layers to have a full contact. They will be partially bonded and form the pattern of "bonded–unbonded–bonded" or "interface–void–interface", which is typical in the micro-scale world [20]. Since the surface roughness in Yu and Suo's model is an ideal sinusoidal variation, Gui et al. developed a more realistic model for the surface topography with the asperities of Gaussian distribution [21]. Yu and Suo's model depicts the nature of the layer interface as "interface–void–interface" type at initial stage. We also assume the two layers are fully-bonded at the final stage, forming a wavy interface similar to Liau's case (shown in Fig. 1c), in which the wavy interface is formed by crystal dislocations [22]. At the same time, the model used here is also able to describe the behavior of the substrate much thicker than the film. The layers are infinite in the x and y directions (the coordinate system is shown in Fig. 1). The sinusoidally varying surface roughness is included in the parameters of the roughness wavelength and misfit gap amplitude. As the S–L model links the interfacial stress states with the middle-surface displacements of the layers [9, 15], and the displacement information is available in the model presented here, we incorporate such interfacial effects at $z = 0$ based on the fact of that the interface layer thickness is very small (for example, the interface layer thickness for a Cu/Si film–substrate composite is on the scale of a nanometer [15]). The interfacial parameter $\frac{G_i}{\eta}$, along with the layers' elastic constants and dimensions determines the normal stress distribution along the thickness. This suggests that for a given composite structure with specified elastic constants and dimensions, the measurements of the surface roughness (before contact/bonding) and those of the normal stress across the thickness (after being fully-bonded) can be used to determine $\frac{G_i}{\eta}$. This is different from the approach by Noyan and Murray et al. [14, 15], which measures the normal stress along the layer *length* to solve for $\frac{G_i}{\eta}$ by Eq. 1. Also by providing the information of the stress normal to the interface, the current model could be used to study the interdiffusion of two bonded layers [23, 24].

Model development

In Fig. 1a and b, the surfaces of the two layers are schematically shown. The layers are infinite in the x–y directions, and sinusoidally varying with a misfit gap amplitude of $2H$ and wavelength of L. t_1 and t_2 are the thickness of the layer 1 and 2 respectively. When the ratio $\frac{H}{L}$ is small, linear elasticity theory applies [19].

Navier's equation is applied as follows, when we assign the displacement field as $(u_1,u_2,u_3) = (u,v,w)$. Navier's equation states:

$$(1-2v)u_{i,jj} + u_{j,ji} = 0. \tag{2}$$

Here $u_{j,ji} = \frac{\partial^2 u_j}{\partial x_i \partial x_j}$. The stress field is:

$$\sigma_{ij} = \frac{E}{1+v}\left[\frac{1}{2}\left(u_{i,j} + u_{j,i}\right) + \frac{v}{1-2v}u_{k,k}\delta_{ij}\right]. \tag{3}$$

E and v are the layers Young's modulus and Poisson's ratio. δ_{ij} is the Kronecker delta. The displacement field is assumed to have the following forms [19]:

$$\begin{aligned} u^i(x,y,z) &= \sin(kx)\cos(ky)f^i(z) \\ v^i(x,y,z) &= \cos(kx)\sin(ky)f^i(z) \\ w^i(x,y,z) &= \cos(kx)\cos(ky)g^i(z), \end{aligned} \tag{4}$$

where superscript $i(i = 1,2)$ stands for the different layers and $k = 2\pi/L$. Originally w^i in Yu and Suo's model [19] contained a rigid body translation term, which has no effect on the stress and is ignored here. The unknown functions f^i and g^i can be solved by substituting Eq. 4 into Eq. 2, which gives the following coupled ordinary differential equations with constant coefficients:

$$\begin{aligned} (1-2v)f'' - 4(1-v)f - g' &= 0 \\ (1-v)g'' - (1-2v)g + f' &= 0, \end{aligned} \tag{5}$$

with $()' = d()/d(kz)$. The equations above have the following solutions:

$$\begin{aligned} f^1(z) &= (a_1 + a_2 kz)e^{\sqrt{2}kz} + (a_3 + a_4 kz)e^{-\sqrt{2}kz} \\ f^2(z) &= (a_5 + a_6 kz)e^{\sqrt{2}kz} + (a_7 + a_8 kz)e^{-\sqrt{2}kz} \\ g^1(z) &= [-\sqrt{2}a_1 + (3 - 4v_1 - \sqrt{2}kz)a_2]e^{\sqrt{2}kz} \\ &\quad + [\sqrt{2}a_3 + (3 - 4v_1 + \sqrt{2}kz)a_4]e^{-\sqrt{2}kz} \\ g^2(z) &= [-\sqrt{2}a_5 + (3 - 4v_2 - \sqrt{2}kz)a_6]e^{\sqrt{2}kz} \\ &\quad + [\sqrt{2}a_7 + (3 - 4v_2 + \sqrt{2}kz)a_8]e^{-\sqrt{2}kz}. \end{aligned} \tag{6}$$

a_i $(i = 1–8)$ are constants to be determined by the boundary conditions. Here v_1 and v_2 are Poisson's ratios of layers 1 and 2.

The four boundary conditions for layer 1 are:

(I)

$$z = t_1, \sigma_{zz}^1 = 0$$

(II)

$$z = t_1, \sigma_{xz}^1 = 0$$

(III)

$$z = 0, w^1 = -\frac{H_1}{2}\cos(kx)\cos(ky)$$

(IV)

$$z = 0, \quad \sigma_{xz}^1 = \frac{G_i}{\eta}[u^1(x,y,\frac{t_1}{2}) - u^2(x,y,-\frac{t_2}{2})]. \tag{7}$$

H_1 is the amplitude of the surface displacement of layer 1 normal to the interface. The first three boundary conditions are same as those in Yu and Suo's [19]. The first two state that on the free surface, the normal and shear stresses are zero. Equation 3 in conjunction with Eq. 4 gives $\sigma_{xz}^i = \frac{E_i}{2(1+\upsilon_i)}(u_z^i + w_z^i) = \frac{E_i}{2(1+\upsilon_i)}\sin(kx)\cos(ky)(\frac{df^i}{dz} - kg)$ and $\sigma_{yz}^i = \frac{E_i}{2(1+\upsilon_i)}(v_z^i + w_y^i) = \frac{E_i}{2(1+\upsilon_i)}\cos(kx)\sin(ky)(\frac{df^i}{dz} - kg)$, which implies that in Eq. 7, to set $\sigma_{xz}^1 = 0$ at $z = t_1$ and $\sigma_{xz}^2 = 0$ at $z = -t_2$ also means $\sigma_{yz}^1 = 0$ at $z = t_1$ and $\sigma_{yz}^2 = 0$ at $z = -t_2$. In the fourth boundary condition, G_i and η are the interface layer shear modulus and thickness, respectively. $u^1(x,y,\frac{t_1}{2})$ and $u^2(x,y,-\frac{t_2}{2})$ are the two x-axis displacements of the two layers' middle-surfaces. And the fourth boundary condition is the interfacial shear stress expression of the S–L model [9, 15]. In Suhir's L–S model [11], a similar expression is given $\sigma_{xz}^1 = \frac{KG_i}{\eta}[u^1(x,y,\frac{t_1}{2}) - u^2(x,y,-\frac{t_2}{2})]$. K is a constant and $K = \frac{1}{3}(\frac{t_1}{G_1} + \frac{t_2}{G_2})$ [10, 13]. G_1,G_2 above are the shear moduli of layer 1 and layer 2, respectively. In this article, we treat $\frac{G_i}{\eta}$ as a parameter whose value varies, in order to study the stress change. In that sense, it does not matter whether such proportionality factor is $\frac{G_i}{\eta}$ or $\frac{KG_i}{\eta}$. Yu and Suo set the shear stress σ_{xz} at interface ($z = 0$) to be zero [19], which is our $\frac{G_i}{\eta} = 0$ case. Similarly, the four boundary conditions for layer 2 are:

(V)

$$z = -t_2, \sigma_{zz}^2 = 0$$

(VI)

$$z = -t_2, \sigma_{xz}^2 = 0$$

(VII)

$$z = 0, w^2 = \frac{H_2}{2}\cos(kx)\cos(ky)$$

(VIII)

$$z = 0, \sigma_{xz}^2 = \frac{G_i}{\eta}[u^1(x,y,\frac{t_1}{2}) - u^2(x,y,-\frac{t_2}{2})]. \tag{8}$$

Here H_2 is the amplitude of the surface displacement of layer 2 normal to the interface. Equations 7 and 8 give the eight boundary conditions needed to solve for the eight unknown $a_i s$. However, it should be noted that H_1 and H_2 are still unknown at this stage. Therefore, the $a_i s$ should be first expressed symbolically by H_1 and H_2, and then by H. The detailed procedure is given in appendix. The two layers are assumed to be fully-bonded as shown in Fig. 1c, and the corresponding physical condition requires H_1 and H_2 to satisfy the following relation [19]:

$$H_1 + H_2 = 2H, \tag{9}$$

which means that the amplitude of relative displacement of the layers is equal to the misfit gap amplitude. And at $z = 0$, the continuity of normal stress of σ_{zz} requires the following equation to be satisfied [19]:

$$\sigma_{zz}^1(z=0) = \sigma_{zz}^2(z=0). \tag{10}$$

Equations 9 and 10 are the two equations to determine H_1 and H_2, and thus $a_i s$.

Results and discussion

In all the cases studied here, E_1 = 129.8 GPa, ν_1 = 0.343 for Cu, E_2 = 162.5 GPa, ν_2 = 0.224 for Si, [15], and L = 1 μm. $G_i = \lambda\frac{E_1+E_2}{2}$ and η = 1 nm. λ is the dimensionless parameter we actually vary during the computation. Although η can be varied, η = 1 nm is chosen in this study because the interface thickness of Cu/Si film–substrate composite structure is of the same order of magnitude. From Eq. 3, the normal stress along the thickness in layer 1 is expressed as

$$\begin{aligned}\sigma_{zz}^1 = \cos(kx)\cos(ky)\phi(z) = \frac{\cos(kx)\cos(ky)E_1}{1+\nu_1} \\ \times [-2ke^{\sqrt{2}kz}a_1 + (2\sqrt{2}k - 2k^2z - 2\sqrt{2}k\nu_1)e^{\sqrt{2}kz}a_2 \\ - 2ke^{-\sqrt{2}kz}a_3 + (-2\sqrt{2}k - 2k^2z + 2\sqrt{2}k\nu_1)e^{-\sqrt{2}kz}a_4].\end{aligned} \tag{11}$$

Clearly, σ_{zz}^1 oscillates periodically in the x and y directions. The following study only presents the variation of the amplitude $\phi(z)$, and all our computation results from Eq. 11 when setting $\lambda = 0$ exactly match those obtained by Yu and Suo [19].

In Fig. 2a, $t_1 = t_2$ = 1 μm and $\frac{H}{L} = \frac{1}{1000}$. The distribution of $\phi(z)$ is shown with λ = 0, 0.05, 0.1, 0.3, 0.5, and 1. When $\lambda = 0$, $\phi(z)$ monotonically decreases from 351.4 MPa at $z = 0$ to 0 MPa at z = 1 μm. For λ = 0.05, $\phi(z)$ decreases from 258.4 MPa at $z = 0$ to 0 MPa at z = 1 μm, and the decrease is still monotonic. However, for λ = 0.1, the curve no longer monotonically decreases. $\phi(z)$ starts with 288.6 MPa at $z = 0$, increases to 607.5 MPa around 0.11 μm, and decreases to 0 at z = 1 μm. For λ = 0.3, 0.5, and 1, $\phi(z)$ becomes monotonically decreasing again. For Fig. 2b, all the parameters are kept same as those in

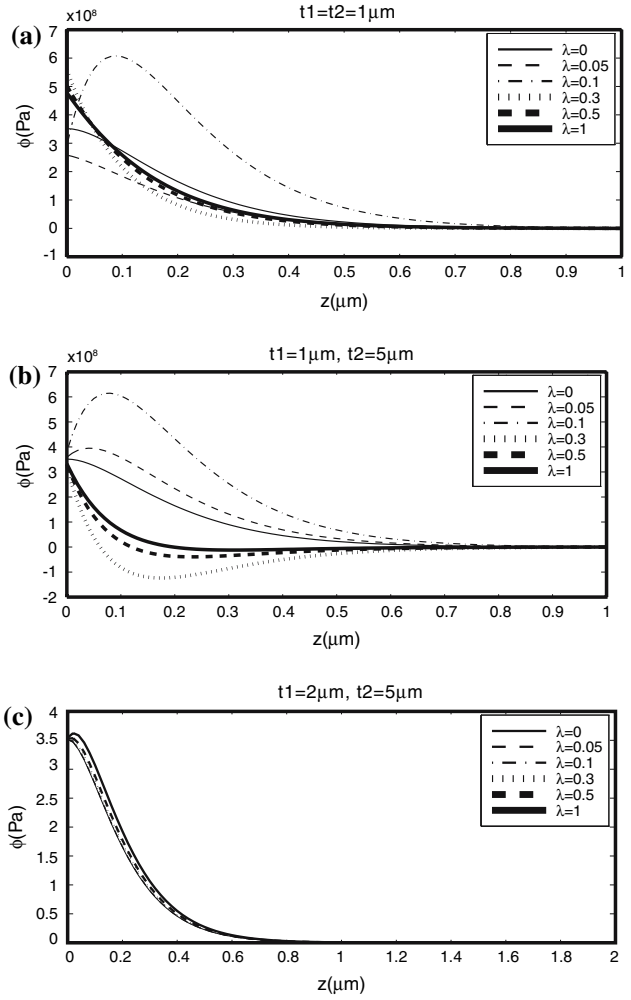

Fig. 2 $\phi(z)$ distributions along the Cu layer thickness for different G_i/η (different λ) and a fixed $H/L = 1/1000$ when (**a**) $t_1 = t_2 = 1$ μm; (**b**) $t_1 = 1$ μm and $t_2 = 5$ μm; (**c**) $t_1 = 2$ μm and $t_2 = 5$ μm

Fig. 2a, except that t_2 is changed to 5 μm. The curve with $\lambda = 0$ is still monotonically decreasing. The curves for $\lambda = 0.05$ and 0.1 are of the increasing–decreasing type. From the curves with $\lambda = 0.3$, 0.5, and 1, a transition from the decreasing–increasing type of curve to the monotonically decreasing type of curve is shown. In this case, there is a little difference in ϕ (0) for all the curves with different λs. In Fig. 2c, t_1 is set to be 2 μm, and all other parameters are same as those in Fig. 2b. Clearly, in Fig. 2c there is a very little difference for the curves with different λs. So, we conclude that the stress distribution along the thickness is sensitive to both layer thickness dimensions from the comparison of Fig. 2b and 2c. Mathematically, the combination of the $e^{\sqrt{2}kz}$ terms associated with a_1 and a_2 and the $e^{-\sqrt{2}kz}$ terms associated with a_3 and a_4 can generate different normal stress profiles as reflected in Fig. 2a, b, and c. Physically, when the layer thickness increases, the ratio of the interface to the (bulk) volume becomes small, which also means that the interface effects become less important. This is the mechanism responsible for the normal stress size-dependent distribution properties, and explains why the normal stress profiles look similar in Fig. 2c when the layers thickness is relatively large. Analogously, both the experimental and theoretical analysis (Eq. 11 [14, 15]) also demonstrate the sample size-dependent sensitivity of the interface layer effects. In the experiment [14], the large difference of the horizontal (parallel to the interface) normal stress distribution between a 3 μm × 3 μm and a 14 μm × 14 μm film is demonstrated.

In Fig. 3, the roughness effect is studied. Two cases, one with $\lambda = 0$, and the other with $\lambda = 0.1$ are compared together. For these two cases, $t_1 = 1$ μm and $t_1 = 5$ μm. $\frac{H}{L}$ is chosen to be 1×10^{-3}, 2×10^{-3}, or 5×10^{-3}. It is shown in Fig. 3 that larger $\frac{H}{L}$ generates a larger magnitude of $\phi(z)$ across the whole thickness, which is physically understandable because a larger $\frac{H}{L}$ requires larger elastic deformation so that the gap can be closed and thus a larger corresponding stress is generated. For the curves with $\lambda = 0.1$, the change in the maximum values is also very significant. However, the parameter $\frac{H}{L}$ does not change type of the curve: for $\lambda = 0$ the curves are all monotonically decreasing, while for $\lambda = 0.1$, the curves all increase and then decrease. The roughness (indicated by $\frac{H}{L}$) offers the source for the normal stress (as the model requires the closing-up). But it is the interfacial shear stress (indicated by λ) that re-distributes the normal stress inside layers. Without the interfacial shear stress, the normal stress distribution pattern can only be monotonically decreasing.

Figure 2a–c demonstrates the thickness-dependence of normal stress distribution due to the interface layer effect,

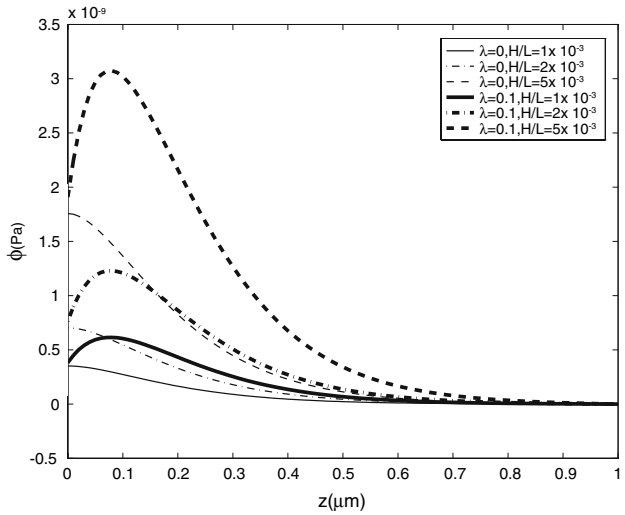

Fig. 3 $\phi(z)$ distributions along the Cu layer thickness for different $\frac{H}{L}$. Here the case with no interface layer effect ($\lambda = 0$) and the case with the interface layer effect (with $\lambda = 0.1$) are compared together. The layer thicknesses ($t_1 = 1$ μm and $t_2 = 5$ μm) are same for both cases

and Fig. 3 demonstrates the roughness influence. The normal stress in the layers depends significantly on the layer thickness, surface roughness, and interface layer conditions.

The changes in the normal stress distribution due to the interface layer conditions could also have a significant impact on the formation, nucleation, and interaction of dislocations [16, 25], penetration of twins across the interface [24], interdiffusion [23, 24], and bonding strength. It is also known that stress inside semiconductor layers can either increase or decrease the charge carrier mobility, which has a direct influence on the electronic properties of the CMOS transistors made by the wafer-bonding technique [16].

It is interesting to compare this work with Liau's [22]. It is noticed that Liau's model predicates that the normal stress distribution along the thickness direction decreases monotonically and exponentially from the interface [22], which is the same scenario as the $\lambda = 0$ cases in Figs. 2 and 3. The expression of Eq. 11 implicates that the normal stress distribution patterns of monotonically decreasing, increasing–decreasing and decreasing–increasing can all exist. Liau's model also assumes that the dislocations are all localized at the interface [22]. However, it can also be rigorously shown that Liau's model assumes that the interface is ideal even with the presence of dislocations [26]. With the accumulation of dislocations or other defects at the interface, the interface strength will be weakened and interfacial slip will be allowed, so the interface should be modeled as a damaged one. The damaged interface along with the layers-thickness dimensions and roughness can significantly alter the normal stress distribution as demonstrated in Figs. 2 and 3. Freund and Suresh's analysis shows that the occurrence of dislocations depends on the (local) strain energy [25], which is directly related to the stress distribution. The normal stress distribution along the thickness direction is usually the dominant one in wafer-bonding materials. As demonstrated by Yu and Suo [19], Liau [22], and this work, for an ideal interface formed by wafer-bonding, the normal stress decreases monotonically from the interface and the maximum stress is at the interface. This is the reason why dislocations in wafer-bonded materials are often localized at the interface and virtually nowhere else [22], if the bonding interface is ideal (or has very high bonding strength). However, the increasing–decreasing normal stress distribution pattern of a damaged interface shifts the maximum stress from the interface into the layer, which directly results in the following consequence: the formation of new dislocations will be most likely to occur inside the layer rather than at the interface. Accordingly, the propagation of dislocation may also be affected because of the different stress field.

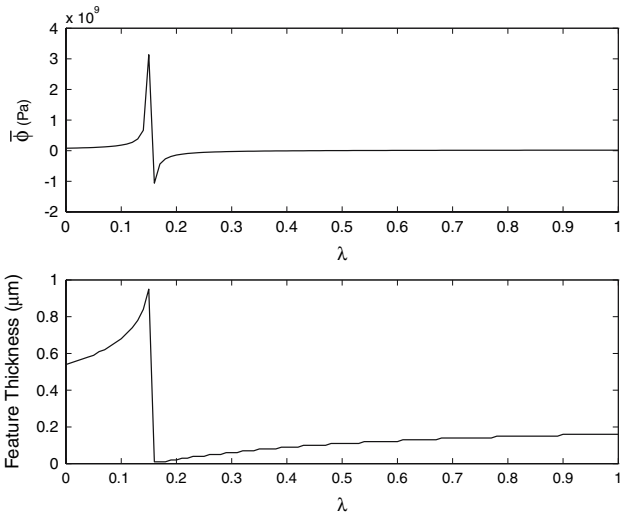

Fig. 4 The average stress ($\overline{\phi}$) inside the Cu layer and the feature thickness as G_i/η (that is, λ) changes in the case of $t_1 = 1$ μm and $t_2 = 5$ μm, as in Fig. 2b

The average $\overline{\phi}$ in layer 1 is defined as follows:

$$\overline{\phi} = \frac{\int_0^{t_1} \phi(z)dz}{t_1}. \tag{12}$$

The feature thickness plotted in Figs. 4 and 5, here, is defined as the length at which $\phi(z)$ is reduced to 5% of $\phi(0)$. The 5% here is an arbitrary number taken to follow Murray and Noyan's definition [15]. $\overline{\phi}$ and the feature thickness together give an overall idea of the stress distribution, namely its magnitude and the degree of stress localization. In Fig. 4, λ is varied, while all other parameters are same as in Fig. 2b. As shown in Fig. 4, both $\overline{\phi}$ and the feature thickness keep increasing before and after $\lambda = 0.15$. At $\lambda = 0.15$, both curves experience a sudden jump. This is also reflected in Fig. 2b. In Fig. 2b, the $\phi(z)$ curves with $\lambda = 0.05$ and 0.1 are the increasing–decreasing type of curves, which have larger $\overline{\phi}$. For the curves with $\lambda = 0.3$, 0.5, and 1, they are either decreasing–increasing or monotonically decreasing types of curve. They decrease much more rapidly, and some parts of $\phi(z)$ are even negative. Therefore, as compared to the increasing–decreasing type of curves, $\phi(z)$s of the curves with $\lambda = 0.3$, 0.5, and 1 reduce much more rapidly as one moves from the interface. This is why the curves with $\lambda = 0.3$, 0.5, and 1 have much smaller $\overline{\phi}$ and feature thickness. This pattern change in the stress distribution is also responsible for the jump in Fig. 4. Figure 5 examines the same case as in Fig. 2c when both films are relatively thick. As shown in Fig. 5, clearly $\overline{\phi}$ increases continuously, but slowly as λ changes. Compared with that of Fig. 4, the variation of $\overline{\phi}$ in Fig. 5 is very small. The feature thickness in Fig. 5 is either 0.54 or 0.56 μm. Although there is a

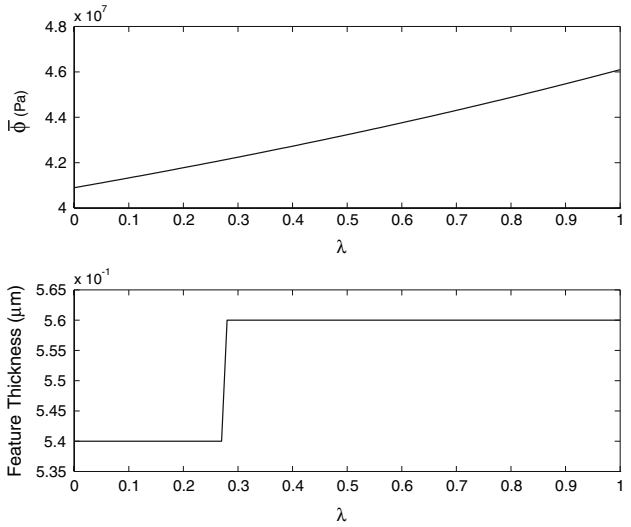

Fig. 5 The average stress $(\bar{\phi})$ inside the Cu layer and the feature thickness as G_i/η (that is, λ) changes in the case of $t_1 = 2$ μm and $t_2 = 5$ μm, as in Fig. 2c

feature thickness jump in Fig. 5, the jump magnitude is quite small compared with that of Fig. 4. Clearly there is no strong pattern change of stress distribution in Fig. 2c. These characteristics in Fig. 5 are also clearly reflected in Fig. 2c. In one word, the differences of the normal stress profiles in Fig. 2b and 2c are responsible for the significant difference between Figs. 4 and 5.

Without the interface effect (i.e., when $\lambda = 0$), the normal stress amplitude along the thickness always keeps monotonically decreasing and the maximum is at $z = 0$ [19]. With the variation of λ, there can be quite different normal stress profiles. The layer thickness, roughness, and $\frac{G_i}{\eta}(G_i = \lambda\frac{E_1+E_2}{2})$ are responsible for the normal stress variation in a given bilayered composite. Here λ is the fitting factor, which indicates the interface layer effect as reflected in Eq. 8. Larger λ indicates larger interfacial shear stress and for a perfect/ideal/no-slip interface, the interfacial shear stress is zero ($\lambda = 0$). The variation of λ in this article represents different interfacial (stress) states. The original S–L model was developed to evaluate how well the two layers are adhered by analyzing the influence of the interfacial slip and stress states [9]. With the availability of the micro-Raman technique for measuring the nonuniform normal stress through the layer thickness [27], it is possible to measure the normal stress and layer surface roughness, and then use the model presented in this article to determine $\frac{G_i}{\eta}$. The bonding strength is usually measured by a method based on crack propagation theory, which does not consider complex stress distribution due to the interface layer effect as analyzed in this article [28]. With experimental information about $\frac{G_i}{\eta}$ and the analysis of the normal stress distribution, it may be possible to obtain a more accurate evaluation of the interface bonding strength.

Concluding remarks

This article presents a model of elastic closing gap that incorporates the interface layer effect. The bonding surfaces are assumed to sinusoidally vary in both the x and y directions. The model directly links the normal stress distribution to the surface roughness and the interfacial parameter $\frac{G_i}{\eta}$ and offers a method to determine the latter value experimentally. The influence of $\frac{G_i}{\eta}$ along with the layers thickness and roughness on the normal stress distribution is studied. As compared to the ideal interface, which can only have the monotonically decreasing pattern of normal stress along the thickness direction, a damaged interface can have one of the following three patterns of normal stress distribution along the thickness direction: (1) monotonically decreasing, (2) increasing–decreasing pattern or (3) a decreasing–increasing pattern. The ideal interface model indicates that the maximum stress locates at the interface, so that the defects such as dislocations are most likely to be formed at the interface. However, the model presented here indicates that the damaged interface along with the thin layer thickness can shift the point of maximum normal stress from the interface into the layer. This results in the consequence that new defects like dislocations are more likely to be formed inside the layer rather than at the interface. However, when the layer thickness is large enough, our model indicates that the damaged interface causes almost the same stress distribution pattern as that of an ideal interface.

The model presented in this article is still an idealized model, which requires the two layers to share the same wavelength. If the two surfaces sufficiently match, this model is a good approximation. Otherwise, a more comprehensive model needs to be developed. The inelastic relaxation and influence of dislocations on the interface layer properties are not included in this model, either.

Acknowledgements The author is thankful for the financial support of the National Natural Science Foundation of China (NSFC, Grant No. 10502050) and the Scientific Research Foundation for the Returned Overseas Chinese Scholars, State Education Ministry.

Appendix

In the boundary conditions as given by Eqs. 7 and 8, the fourth and eighth are equivalent to the following two:

$$\sigma_{xz}^1(z=0) - \sigma_{xz}^2(z=0) = 0$$

$$\sigma_{xz}^1(z=0) + \sigma_{xz}^2(z=0) = \frac{2G_i}{\eta}[u^1(z=\frac{t_1}{2}) - u^2(z=-\frac{t_2}{2})].$$

We arrange them in the last two rows of the following matrix form:

$$\begin{bmatrix} m_{11} & m_{12} & m_{13} & m_{14} & 0 & 0 & 0 & 0 \\ m_{21} & m_{22} & m_{23} & m_{24} & 0 & 0 & 0 & 0 \\ m_{31} & m_{32} & m_{33} & m_{34} & 0 & 0 & 0 & 0 \\ 0 & 0 & 0 & 0 & m_{45} & m_{46} & m_{47} & m_{48} \\ 0 & 0 & 0 & 0 & m_{55} & m_{56} & m_{57} & m_{58} \\ 0 & 0 & 0 & 0 & m_{65} & m_{66} & m_{67} & m_{68} \\ m_{71} & m_{72} & m_{73} & m_{74} & m_{75} & m_{76} & m_{77} & m_{78} \\ m_{81} & m_{82} & m_{83} & m_{84} & m_{85} & m_{86} & m_{87} & m_{88} \end{bmatrix} \begin{pmatrix} a_1 \\ a_2 \\ a_3 \\ a_4 \\ a_5 \\ a_6 \\ a_7 \\ a_8 \end{pmatrix} = \begin{pmatrix} 0 \\ 0 \\ -\frac{H_1}{2} \\ 0 \\ 0 \\ \frac{H_2}{2} \\ 0 \\ 0 \end{pmatrix} \tag{13}$$

With m_{ij} s given as:

$m_{11} = -2ke^{\sqrt{2}kt_1}$,
$m_{12} = k(2\sqrt{2} - 2kt_1 - 2\sqrt{2}v_1)e^{\sqrt{2}kt_1}$,
$m_{13} = -2ke^{-\sqrt{2}kt_1}$,
$m_{14} = k(-2\sqrt{2} - 2kt_1 + 2\sqrt{2}v_1)e^{-\sqrt{2}kt_1}$
$m_{21} = 2\sqrt{2}ke^{\sqrt{2}kt_1}$,
$m_{22} = k(-2 + 4v_1 + 2\sqrt{2}kt_1)e^{\sqrt{2}kt_1}$,
$m_{23} = -2\sqrt{2}ke^{-\sqrt{2}kt_1}$,
$m_{24} = k(-2 + 4v_1 - 2\sqrt{2}kt_1)e^{-\sqrt{2}kt_1}$
$m_{31} = -\sqrt{2}$, m_{32} = 3–4v_1,
$m_{33} = \sqrt{2}$,
m_{34} = 3–4v_1
$m_{45} = -2ke^{-\sqrt{2}kt_2}$,
$m_{46} = k(2\sqrt{2} + 2kt_2 - 2\sqrt{2}v_2)e^{-\sqrt{2}kt_2}$,
$m_{47} = -2ke^{\sqrt{2}kt_2}$,
$m_{48} = k(-2\sqrt{2} + 2kt_2 + 2\sqrt{2}v_2)e^{\sqrt{2}kt_2}$
$m_{55} = 2\sqrt{2}ke^{-\sqrt{2}kt_2}$,
$m_{56} = k(-2 + 4v_2 - 2\sqrt{2}kt_2)e^{-\sqrt{2}kt_2}$,
$m_{57} = -2\sqrt{2}ke^{\sqrt{2}kt_2}$,
$m_{58} = k(-2 + 4v_2 + 2\sqrt{2}kt_2)e^{\sqrt{2}kt_2}$
$m_{65} = -\sqrt{2}$, m_{66} = 3–4v_2,
$m_{67} = \sqrt{2}$, m_{68} = 3–4v_2,
$m_{71} = \sqrt{2}\frac{E_1(1+v_2)}{E_2(1+v_1)}$,
$m_{72} = (-1 + 2v_1)\frac{E_1(1+v_2)}{E_2(1+v_1)}$,
$m_{73} = -\sqrt{2}\frac{E_1(1+v_2)}{E_2(1+v_1)}$,
$m_{74} = (-1 + 2v_1)\frac{E_1(1+v_2)}{E_2(1+v_1)}$,
$m_{75} = -\sqrt{2}$,
m_{76} = 1–2v_2,
$m_{77} = \sqrt{2}$,
m_{78} = 1–2v_2
$m_{81} = \frac{\sqrt{2}E_1k}{1+v_1} - \frac{2G_i}{\eta}e^{\frac{\sqrt{2}}{2}kt_1}$,
$m_{82} = \frac{E_1k(-1+2v_1)}{1+v_1} - \frac{G_ikt_1}{\eta}e^{\frac{\sqrt{2}}{2}kt_1}$,
$m_{83} = \frac{-\sqrt{2}E_1k}{1+v_1} - \frac{2G_i}{\eta}e^{\frac{-\sqrt{2}}{2}kt_1}$,
$m_{84} = \frac{E_1k(-1+2v_1)}{1+v_1} - \frac{G_ikt_1}{\eta}e^{\frac{-\sqrt{2}}{2}kt_1}$,
$m_{85} = \frac{\sqrt{2}E_2k}{1+v_2} + \frac{2G_i}{\eta}e^{\frac{-\sqrt{2}}{2}kt_2}$,
$m_{86} = \frac{E_2k(-1+2v_2)}{1+v_2} - \frac{G_ikt_2}{\eta}e^{\frac{-\sqrt{2}}{2}kt_2}$,
$m_{87} = \frac{-\sqrt{2}E_2k}{1+v_2} + \frac{2G_i}{\eta}e^{\frac{\sqrt{2}}{2}kt_2}$,
$m_{88} = \frac{E_2k(-1+2v_2)}{1+v_2} - \frac{G_ikt_2}{\eta}e^{\frac{\sqrt{2}}{2}kt_2}$

The strategy of solving Eq. 13 is to express a_1, a_2, a_3 via a_4 and a_5, a_6, a_7 via a_8 first, and then substitute them into the last two equations of Eq. 13 to solve a_4 and a_8. Therefore, we have

$$a_1 = \frac{\begin{vmatrix} V_1 & m_{12} & m_{13} \\ V_2 & m_{22} & m_{23} \\ V_3 & m_{32} & m_{33} \end{vmatrix}}{D} = \frac{k_1}{D}a_4 - \frac{H_1}{2D}(m_{12}m_{23} - m_{13}m_{22}), \tag{14}$$

$$a_2 = \frac{\begin{vmatrix} m_{11} & V_1 & m_{13} \\ m_{21} & V_2 & m_{23} \\ m_{31} & V_3 & m_{33} \end{vmatrix}}{D} = \frac{k_2}{D}a_4 + \frac{H_1}{2D}(m_{11}m_{23} - m_{13}m_{21}), \tag{15}$$

and

$$a_3 = \frac{\begin{vmatrix} m_{11} & m_{12} & V_1 \\ m_{21} & m_{22} & V_2 \\ m_{31} & m_{23} & V_3 \end{vmatrix}}{D} = \frac{k_3}{D}a_4 + \frac{H_1}{2D}(m_{12}m_{21} - m_{11}m_{22}), \tag{16}$$

here D, V_1, V_2, and V_3 are defined as

$$D = \begin{vmatrix} m_{11} & m_{12} & m_{13} \\ m_{21} & m_{22} & m_{23} \\ m_{31} & m_{32} & m_{33} \end{vmatrix}, V_1 = -m_{14}a_4,\ V_2 = -m_{24}a_4,$$
$$V_3 = -\frac{H_1}{2} - m_{34}a_4.$$

And k_1, k_2, and k_3 are k_1 = $-m_{14}(m_{22}m_{33}-m_{23}m_{32})+m_{24}(m_{12}m_{33}-m_{13}m_{32})-m_{34}(m_{12}m_{23}-m_{13}m_{22})$, $k_2 = m_{14}(m_{21}m_{33}-m_{23}m_{31})-m_{24}(m_{11}m_{33}-m_{13}m_{31}) + m_{34}(m_{11}m_{23}-m_{13}m_{21})$, $k_3 = m_{14}(m_{22}m_{31}-m_{21}m_{32})-m_{24}(m_{12}m_{31}-m_{11}m_{32}) + m_{34}(m_{12}m_{21}-m_{11}m_{22})$.

a_5, a_6, and a_7 are:

$$a_5 = \frac{\begin{vmatrix} V_5 & m_{46} & m_{47} \\ V_6 & m_{56} & m_{57} \\ V_7 & m_{66} & m_{67} \end{vmatrix}}{J} = \frac{l_1}{J}a_8 + \frac{H_2}{2J}(m_{46}m_{57} - m_{47}m_{56}), \tag{17}$$

$$a_6 = \frac{\begin{vmatrix} m_{45} & V_5 & m_{47} \\ m_{55} & V_6 & m_{57} \\ m_{65} & V_7 & m_{67} \end{vmatrix}}{J} = \frac{l_2}{J}a_8 - \frac{H_2}{2J}(m_{45}m_{57} - m_{47}m_{55}), \tag{18}$$

and

$$a_7 = \frac{\begin{vmatrix} m_{45} & m_{46} & V_5 \\ m_{55} & m_{56} & V_6 \\ m_{65} & m_{66} & V_7 \end{vmatrix}}{J} = \frac{l_3}{J}a_8 - \frac{H_2}{2J}(m_{46}m_{55} - m_{45}m_{56}), \tag{19}$$

with J, V_5, V_6 and V_7 defined as

$$J = \begin{vmatrix} m_{45} & m_{46} & m_{47} \\ m_{55} & m_{56} & m_{57} \\ m_{65} & m_{66} & m_{67} \end{vmatrix}, \; V_5 = -m_{48}a_8, \; V_6 = -m_{58}a_8,$$
$$V_7 = \frac{H_2}{2} - m_{68}a_8.$$

l_1, l_2, and l_3 are $l_1 = -m_{48}(m_{56}m_{67}-m_{57}m_{66}) + m_{58}(m_{46}m_{67}-m_{47}m_{66}) - m_{68}(m_{46}m_{57}-m_{47}m_{56})$, $l_2 = m_{48}(m_{55}m_{67}-m_{57}m_{65}) - m_{58}(m_{45}m_{67}-m_{47}m_{65}) + m_{68}(m_{45}m_{57}-m_{47}m_{55})$.

And $l_3 = m_{48}(m_{56}m_{65}-m_{55}m_{66}) - m_{58}(m_{46}m_{65}-m_{45}m_{66}) + m_{68}(m_{46}m_{55}-m_{45}m_{56})$.

Substitution of the expressions of a_1, a_2, $a_3$in Eqs. 14, 15, 16 and a_5, a_6, a_7 in Eqs.17, 18, 19 into the last two equations of Eq. 13 gives following equations of a_4 and a_8:

$$\begin{cases} M_{11}a_4 + M_{12}a_8 = \frac{H_1}{2D}\alpha_1 + \frac{H_2}{2J}\alpha_2 \\ M_{21}a_4 + M_{22}a_8 = \frac{H_1}{2D}\gamma_1 + \frac{H_2}{2J}\gamma_2 \end{cases}, \tag{20}$$

with M_{ij}s defined as $M_{11} = \frac{m_{71}k_1 + m_{72}k_2 + m_{73}k_3}{D} + m_{74}$, $M_{12} = \frac{m_{75}l_1 + m_{76}l_2 + m_{77}l_3}{J} + m_{78}$, and $M_{21} = \frac{m_{81}k_1 + m_{82}k_2 + m_{83}k_3}{D} + m_{84}$, $M_{22} = \frac{m_{85}l_1 + m_{86}l_2 + m_{87}l_3}{J} + m_{88}$.

And α_1 and α_2 are defined as

$$\alpha_1 = m_{71}(m_{12}m_{23} - m_{13}m_{22}) - m_{72}(m_{11}m_{23} - m_{13}m_{21}) - m_{73}(m_{12}m_{21} - m_{11}m_{22})$$

and

$$\alpha_2 = -m_{75}(m_{46}m_{57} - m_{47}m_{56}) + m_{76}(m_{45}m_{57} - m_{47}m_{55}) + m_{77}(m_{46}m_{55} - m_{45}m_{56}).$$

γ_1 and γ_2 are

$$\gamma_1 = m_{81}(m_{12}m_{23} - m_{13}m_{22}) - m_{82}(m_{11}m_{23} - m_{13}m_{21}) - m_{83}(m_{12}m_{21} - m_{11}m_{22}),$$

and

$$\gamma_2 = -m_{85}(m_{46}m_{57} - m_{47}m_{56}) + m_{86}(m_{45}m_{57} - m_{47}m_{55}) + m_{87}(m_{46}m_{55} - m_{45}m_{56}).$$

a_4 and a_8 are solved as

$$a_4 = A_1H_1 + A_2H_2, a_8 = B_1H_1 + B_2H_2, \tag{21}$$

with A_i and B_i (i = 1, 2) given as

$$A_1 = \frac{\alpha_1M_{22} - \gamma_1M_{12}}{2D(M_{11}M_{22} - M_{12}M_{21})}, A_2 = \frac{\alpha_2M_{22} - \gamma_2M_{12}}{2J(M_{11}M_{22} - M_{12}M_{21})}.$$

and

$$B_1 = \frac{\gamma_1M_{11} - \alpha_1M_{21}}{2D(M_{11}M_{22} - M_{12}M_{21})}, B_2 = \frac{\gamma_2M_{11} - \alpha_2M_{21}}{2J(M_{11}M_{22} - M_{12}M_{21})}.$$

Substitute the above solution of a_8 and a_4 into Eqs. 14, 15, and 16, and 17, 18, and 19, we have

$$a_1 = C_1H_1 + C_2H_2, a_2 = F_1H_1 + F_2H_2, a_3 = I_1H_1 + I_2H_2$$
$$a_5 = P_1H_1 + P_2H_2, a_6 = Q_1H_1 + Q_2H_2, a_7 = R_1H_1 + R_2H_2, \tag{22}$$

with

$$C_1 = \frac{k_1}{D}A_1 - \frac{m_{12}m_{23} - m_{13}m_{22}}{2D}, C_2 = \frac{k_1}{D}A_2,$$
$$F_1 = \frac{k_2}{D}A_1 + \frac{m_{11}m_{23} - m_{13}m_{21}}{2D}, F_2 = \frac{k_2}{D}A_2,$$

$$I_1 = \frac{k_3}{D}A_1 + \frac{m_{12}m_{21} - m_{11}m_{22}}{2D}, I_2 = \frac{k_3}{D}A_2, P_1 = \frac{l_1}{J}B_1,$$
$$P_2 = \frac{l_1}{J}B_2 + \frac{m_{46}m_{57} - m_{47}m_{56}}{2J},$$

and

$$Q_1 = \frac{l_2}{J}B_1, Q_2 = \frac{l_2}{J}B_2 - \frac{m_{45}m_{57} - m_{47}m_{55}}{2J}, R_1 = \frac{l_3}{J}B_1,$$
$$R_2 = \frac{l_3}{J}B_2 - \frac{m_{46}m_{55} - m_{45}m_{56}}{2J}$$

Equations 9 and 10 result in the following two equations:

$$\begin{cases} H_1 + H_2 = 2H \\ H_1 + rH_2 = 0 \end{cases}. \quad (23)$$

Here r is defined as

$$r = \frac{-\beta C_2 + \sqrt{2}\beta(1-v_1)F_2 - \beta I_2 - \sqrt{2}(1-v_1)A_2 + P_2 - \sqrt{2}(1-v_2)Q_2 + R_2 + \sqrt{2}(1-v_2)B_2}{-\beta C_1 + \sqrt{2}\beta(1-v_1)F_1 - \beta I_1 - \sqrt{2}(1-v_1)A_1 + P_1 - \sqrt{2}(1-v_2)Q_1 + R_1 + \sqrt{2}(1-v_2)B_1},$$

with

$$\beta = \frac{E_1(1+v_2)}{E_2(1+v_1)}$$

Therefore, H_1 and H_2 are solved as follows

$$H_1 = \frac{-2rH}{1-r}, H_2 = \frac{2H}{1-r}. \quad (24)$$

Substitution of the above solution of H_1 and H_2 into Eqs. 21 and 22 gives the solutions of all a_is.

References

1. Pipes RB, Pagano NJ (1970) J Compos Mater 4:538
2. Pipes RB, Moiré IM (1971) J Compos Mater 5:255
3. Pagano NJ (1978) Int J Solids Struct 14:385
4. Pagano NJ (1978) Int J Solids Struct 14:401
5. Wang SS, Choi I (1982) J Appl Mech 49:541
6. Wang SS, Choi I (1982) J Appl Mech 49:549
7. Hu SM (1979) J Appl Phys 50:4661
8. Hu SM (1991) J Appl Phys 70:R53
9. Chen WT, Nelson CW (1979) IBM J Res Develop 23:179
10. Suhir E (1986) J Appl Mech 53:657
11. Suhir E (1989) J Appl Mech 56:595
12. Timoshenko S (1925) J Opt Soc Am 11:233
13. Ru CQ (2002) J Electron Packag 124:141
14. Noyan IC, Murray CE, Chey JS, Goldsmith CC (2004) Appl Phys Lett 85:724
15. Murray CE, Noyan IC (2002) Philos Mag A 82:3087
16. Maszara WP, Jiang BL, Yamada A, Rozgonyi GA, Baumgart H, de Kock AJR (1990) J Appl Phys 69:257
17. Stengl R, Mitani K, Lehmann V, Gösele U (1989) Proc. 1989 IEEE SOS/SOI Tech. Conf., Stateline, Nevada, October 3–5, 1989, IEEE Catalog number 89CH2796–1(1989) 123
18. Tong QY, Gösele U (1995) J Electrochem Soc 142:3975
19. Yu HH, Suo Z (1998) J Mech Phys Solids 46:829
20. Kendall K (2001) Molecular adhesion and its application: the sticky universe. Kluwer Academic /Plenum Publishers, NY, p 28
21. Gui C, Elwenspoek M, Tas N, Gardeniers JGE (1999) J Appl Phys 85:7448
22. Liau ZL (1997) Phys Rev B 55:12899
23. Lee WG, Woo SI (1997) J Mater Sci 32:815
24. Chen KN, Fan A, Reif R (2002) J Mater Sci 37:3441
25. Freund LB, Suresh S (2003) Thin film materials: stress, defect formation and surface evolution. Cambridge University Press, UK
26. Zhang Y (2007) J Phy D Appl Phy 40:1118
27. Pinard K, Jain SC, Willander M, Atkinson A, Maes HE, Van Overstraeten R (1998) J Appl Phys 84:2507
28. Maszara WP, Goetz G, Caviglia A, McKitterick JB (1988) J Appl Phys 64:4943